
AASAE: Augmentation-Augmented Stochastic Autoencoders

William Falcon^{1,2*} Ananya Harsh Jha^{1*} Teddy Koker^{1†} Kyunghyun Cho^{2,3}

¹ Grid AI Labs

² New York University

³ CIFAR Fellow

{will, ananya}@grid.ai

Abstract

Recent methods for self-supervised learning can be grouped into two paradigms: contrastive and non-contrastive approaches. Their success can largely be attributed to data augmentation pipelines which generate multiple views of a single input that preserve the underlying semantics. In this work, we introduce augmentation-augmented stochastic autoencoders (AASAE), yet another alternative to self-supervised learning, based on autoencoding. We derive AASAE starting from the conventional variational autoencoder (VAE), by replacing the KL divergence regularization, which is agnostic to the input domain, with data augmentations that explicitly encourage the internal representations to encode domain-specific invariances and equivariances. We empirically evaluate the proposed AASAE on image classification, similar to how recent contrastive and non-contrastive learning algorithms have been evaluated. Our experiments confirm the effectiveness of data augmentation as a replacement for KL divergence regularization. The AASAE outperforms the VAE by 30% on CIFAR-10, 40% on STL-10 and 45% on Imagenet. On CIFAR-10 and STL-10, the results for AASAE are largely comparable to the state-of-the-art algorithms for self-supervised learning^{**}.

1 Introduction

The goal of self-supervised learning (SSL) [14] is to learn good representations from unlabeled examples. A good representation is often defined as the one that reflects underlying class structures well. The quality of a representation obtained from SSL is evaluated by measuring downstream classification accuracy on a labelled dataset. In recent years, two families of approaches have emerged as the state-of-the-art for SSL: contrastive and non-contrastive learning.

At its core, a contrastive learning algorithm stochastically creates two views from each training example, called positive and anchor examples, and selects one of the other training examples as a negative [2, 53, 9, 7]. The positive and anchor examples are brought closer in the representation space, while the negative example is pushed away from the anchor. This definition of contrastive loss brings in two interconnected issues. First, there is no principled way to choose negative examples, and hence these negatives are chosen somewhat arbitrarily each time. Second, the contrastive loss function is not decomposed over training examples because negative examples come from other training examples.

*equal contribution

†work done while at Grid AI Labs

**implementation available on <https://github.com/gridai-labs/aavae>

Partly to address these limitations, recent studies have proposed non-contrastive approaches that have removed the need for negative examples [28, 5, 61]. These approaches avoid the necessity of explicit negatives by constraining or regularizing dataset-level statistics of internal representation [61, 6, 22]. Dataset-level statistics, which are intractable to compute, are instead approximated using a minibatch of training examples. This often results in the need of large minibatches. Also, the use of batch-level statistics means that non-contrastive losses are not decomposable as well.

Despite the apparent differences between these two families of algorithms, they all recognize the importance of and rely heavily on data augmentation as a way of incorporating domain knowledge. For instance, Chen et al. [7] have highlighted that the downstream accuracy after finetuning varied between 2.6% and 69.3% on ImageNet [13], depending on the choice of data augmentation. This is perhaps unsurprising since the importance of domain knowledge has been reported in various domains beyond computer vision. In reinforcement learning, Kostrikov et al. [39] and Raileanu et al. [49] have shown the benefit of adding domain information via pixel-level data augmentation in continuous control. In natural language processing, Ng et al. [44] demonstrate the effectiveness of domain-specific augmentation by using a pretrained denoising autoencoder to build a robust classifier.

A variational autoencoder (VAE) implements a latent variable model using a composition of two neural networks. A neural net decoder maps a latent variable configuration to an observation, and a neural net encoder approximately infers the latent variable configuration given the observation [38]. It is often trained to maximize the variational lowerbound or its variant [38, 33]. Careful inspection of this learning objective shows two parts: autoencoding and latent-space regularization. Autoencoding ensures that there is an approximately one-to-one mapping between individual inputs and internal representations. This prevents the collapse of internal representations onto a single point, similar to what negative examples in contrastive learning and regularization of batch-level statistics in non-contrastive learning do. Latent-space regularization, on the other hand, ensures that the internal representation is arranged semantically in a compact subset of the space. It is often done by minimizing the KL divergence [41] from the approximate posterior, returned by the encoder, to the prior distribution and adding noise to the representation during training (i.e., sampling from the approximate posterior). This performs a role similar to that of data augmentation in contrastive and non-contrastive approaches but is different in a way that it is agnostic to the input domain.

Based on these observations: (1) the importance of data augmentations and (2) variational autoencoders for representation learning, we propose a third family of self-supervised learning algorithms in which we augment variational autoencoders with data augmentation. We refer to this family of models as Augmentation-Augmented Stochastic Autoencoders (AASAE). In AASAEs, we replace the usual KL-divergence [41] term in ELBO [38] with a denoising criterion [56, 57] based on domain-specific data augmentation. We hypothesize that this new approach allows the representations learned by AASAEs to encode domain-specific data invariances and equivariances. The resulting model offers a few advantages over the existing contrastive and non-contrastive methods. First, the loss function is not dependent on the batch-level statistics, which we suspect enables us to use smaller minibatches. Second, the AASAE does not necessitate an arbitrary choice of negative sampling strategy.

We pretrain AASAEs on image datasets: CIFAR-10 [40], STL-10 [11] and Imagenet [13], and as is the norm with other recently proposed approaches [26, 7, 5], we evaluate them on classification tasks corresponding to the dataset using a single linear layer without propagating gradients back to the encoder. We find that our autoencoding-based method gives a downstream classification performance comparable to the current state-of-the-art SSL methods, with 87.14% accuracy on CIFAR-10 and 84.72% on STL-10. On Imagenet, the AASAE outperforms the carefully crafted pretext tasks for SSL, such as Colorization [62], Jigsaw [45] and Rotation [23], demonstrating that designing such complex pretext tasks is unnecessary. As anticipated from our formulation, representation learned by the AASAE is robust to the choice of hyperparameters, including minibatch size, latent space dimension, and the network architecture of the decoder. Our observations strongly suggest that autoencoding is a viable third family of self-supervised learning approach in addition to contrastive and non-contrastive learning.

2 Self-Supervised Learning

Self-supervised learning (SSL) aims to derive training signal from the implicit structure present within data [14]. This enables SSL methods to leverage large unlabeled datasets to learn representations

[27] which can then be used to solve downstream tasks, such as classification and segmentation, for which it is often expensive to collect a large number of annotations. Here, we summarize quite a few variations of this approach proposed over the last few years.

2.1 Pretext tasks

Pretext tasks are designed to train a neural network to predict a non-trivial but easily applicable transformation applied to the input. For example, Gidaris et al. [23] randomly rotate an input image by 0° , 90° , 180° , or 270° and train a network to predict the angle of rotation. The colorization pretext task [62] creates a training signal by converting RGB images to grayscale and training a network to restore the removed color channels. Image inpainting [48] learns representations by training an encoder-decoder network to fill in artificially-occluded parts of an image. Both jigsaw [45] and relative patch prediction [17] tasks divide an input image into patches. The jigsaw task [45] shuffles the spatial ordering of these patches and trains a network to predict the correct order. In contrast, relative patch prediction [17] selects two patches of an image and asks the network to predict their relative spatial positions. More recently, Doersch and Zisserman [16] combined various pretext tasks into a single method. Goyal et al. [26] have, however, shown that training neural network backbones using pretext tasks often does not capture representations invariant to pixel-space perturbations. Consequently, these representations perform poorly on downstream tasks while they solve the original pretext task well.

2.2 Contrastive learning

Between the two major families of state-of-the-art methods for self-supervised learning, we discuss the one based on the so-called contrastive loss function [29]. The contrastive loss is defined such that when minimized, the representations of similar input points are pulled towards each other, while those of dissimilar input points are pushed away from each other. The contrastive loss has its roots in linear discriminant analysis [21] and is closely related to the triplet loss [58]. Recent approaches in contrastive learning are characterized by the InfoNCE loss proposed by Oord et al. [47]. CPC uses InfoNCE as a lower bound of mutual information (MI) and maximizes this lowerbound, by using negative examples. Deep InfoMax [34] similarly proposes to use the idea of maximizing MI while considering global and local representations of an image. Hjelm et al. [34] tested three bounds on MI: Donsker-Varadhan [18], Jensen-Shannon [46], and InfoNCE [47], and found that the InfoNCE objective resulted in the best downstream classification accuracies. Since then, several more advances in contrastive self-supervised learning have happened, such as AMDIM [2] and CMC [53], both of which focus on using multiple views of each image. Hénaff et al. [32] extend CPC with an image patch prediction task, and YADIM [19] combines these ideas of augmentation and InfoNCE loss from both CPCv2 [32] and AMDIM [2] under a single framework.

The success of contrastive learning comes from using a large number of negative examples. Misra and van der Maaten [43] empirically demonstrate with PIRL the benefits of using a large number of negative examples for downstream task performance. PIRL uses a momentum-updated memory bank [60] to provide this large cache of negatives. Memory bank models [60, 43] need to store and update representations for each data point and hence cannot be scaled up efficiently. To remove the dependence on memory bank, MoCo [31, 9] instead introduces a momentum-updated encoder and a comparatively smaller queue of representations to set up positive and negative pairs for contrastive learning. SimCLR [7] removes memory banks and momentum-updated encoders and scales up the batch size to provide a large number of negatives from within each mini-batch. The necessity of a large quantity of negatives for the contrastive loss function to work well proves to be a major challenge in scaling up these methods.

2.3 Non-contrastive approaches

The second family consists of non-contrastive learning algorithms that aim to learn good representations without negative samples by relying on data-level or batch-level statistics. These algorithms can be classified into two groups: clustering-based [4, 1, 5] and distillation-based [28, 8, 24, 6] approaches. A more recently proposed method Barlow Twins [61] does not fall under either group.

Clustering-based methods, such as DeepCluster [4], generate pseudo-labels for training examples by grouping them in the latent space of a neural network. The pseudo-labels are then used to train the

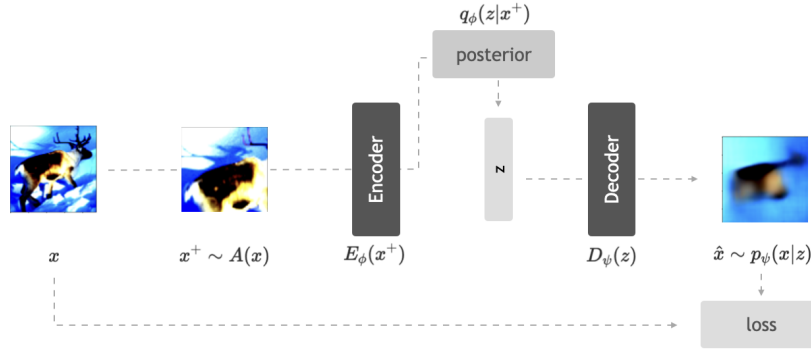


Figure 1: AASAE: The input to the model is an augmented view of $x^+ \sim A(x)$, the target is the original input x . The loss is the reconstruction term of the ELBO (Eq. 3) without the KL-divergence.

neural network. These two steps are repeated several times. Like any classical clustering algorithm, such as k -means, this approach exhibits degenerate solutions and requires additional regularization to avoid these solutions. One such degenerate solution is to put all examples into a single cluster. SeLA [1] regularizes the clustering process with the Sinkhorn-Knopp algorithm [12], encouraging training examples to be equally distributed across the clusters. Caron et al. [5] extend this approach to use data augmentations and online soft assignments of training examples.

Instead of clustering examples, distillation-based approaches [52] rely on having a separate neural network called a teacher network to provide a student network with a target class for each training example. Similar to clustering-based approaches above, this strategy also exhibits trivial solutions, such as the teacher and student networks being constant functions without proper regularization. BYOL [28, 50, 55], and its simpler variant called SimSIAM [8], rely on asymmetry in the network architecture between the teacher and student to avoid such degeneracy. To simplify things, SimSIAM [8] goes one step further than BYOL [28] and removes the momentum-based updates for the teacher network. On the other hand, DINO [6] retains the momentum-based updates for the teacher network, replaces the architectural asymmetry with centering of representations of examples within each minibatch, and demonstrates that these techniques combined with a tempered softmax are sufficient regularizers to avoid degeneracy.

Barlow Twins [61] stands out as an alternative to these two families of approaches. It mixes three principles; (1) batch-level statistics, (2) data augmentation, and (3) whitening (redundancy reduction). At each update, Barlow Twins [61] normalizes the representations of the training examples within each minibatch to have zero-mean and unit-variance along each dimension. It then tries to maximize the cosine similarity between the representation vectors coming out of a pair of samples drawn from a stochastic data augmentation pipeline applied over a single training example. Finally, Barlow Twins [61] minimizes the cross-correlation between different coordinates of these vector representations, which amounts to reducing redundancy at the second-order moment. A similar approach has also been proposed by Bardes et al. [3].

3 Augmentation-Augmented Stochastic Autoencoders

Here we revive the idea of autoencoding as a third paradigm for self-supervised learning, in addition to contrastive and non-contrastive learning, which are described in the previous section. In particular, we start from variational autoencoders (VAEs) [38] to build a new self-supervised learning algorithm for representation learning. There are three mechanisms by which a VAE captures good representations of data; (1) autoencoding, (2) sampling at the intermediate layer, and (3) minimizing KL divergence [41] from the approximate posterior to the prior distribution, all of which are largely domain-agnostic. We thus introduce domain-specific knowledge by replacing the first mechanism (autoencoding) with denoising [56, 57] via data augmentation. Furthermore, we remove the third mechanism as we expect KL divergence minimization to be redundant in representation learning. In this section, we explain the original VAE and then carefully describe our proposal of augmentation-augmented stochastic autoencoder.

3.1 Training a VAE with the evidence lowerbound (ELBO)

We describe algorithms in this section with the assumption that we are working with images, as has been often done with recent work in self-supervised learning [47, 34, 7]. Hence, let the input x be an image, where $x \in \mathbb{R}^{c \times h \times w}$ with c color channels of height h and width w . The VAE then uses a continuous latent variable $z \in \mathbb{R}^d$ to map the high dimensional input distribution, as $p(x) = \int_z p(x|z)p(z)dz$.

It is however intractable to marginalize z in general, and instead we use a tractable lowerbound to the average log-probability of the training examples. Let $q_\phi(z|x)$ be an approximate posterior distribution to the intractable distribution $p(z|x)$, parametrized by the output of the encoder $E_\phi(x)$. $p_\psi(x|z)$ is a probability distribution over the input x , parametrized by the output of the decoder $D_\psi(z)$. The *variational lowerbound* (ELBO) [38] to the log-marginal probability $\log p(x)$ is

$$\log p(x) \geq \tilde{\mathcal{L}}(x) = \mathbb{E}_{z \sim q_\phi(z|x)} [\log p_\psi(x|z) + \beta (\log p(z) - \log q_\phi(z|x))]. \quad (1)$$

The VAE is then trained by minimizing

$$J_{\text{VAE}}(\phi, \psi) = -\frac{1}{N} \sum_{n=1}^N \tilde{\mathcal{L}}(x^n), \quad (2)$$

where x^n is the n -th training example.

The first term in Eq. 1 serves two purposes. First, it minimizes the reconstruction error, which encourages the intermediate representation of the VAE to be more or less unique for each observation. In other words, it ensures that the internal representations of the inputs do not collapse onto each other. The second purpose, expressed as the expectation over the approximate posterior, is to make the representation space smooth by ensuring a small perturbation to the representation does not alter the decoded observation dramatically.

The second term, the KL divergence [41] from the approximate posterior to the prior, serves a single purpose. It ensures that the representation of any observation under the data distribution is highly likely under the prior distribution. The prior distribution is often constructed to be a standard Normal, implying that the probability mass is highly concentrated near the origin (though not necessarily on the origin). This ensures that the representations from observations are tightly arranged according to their semantics, without relying on any domain knowledge.

3.2 Augmentation-augmented stochastic autoencoder

The AASAE removes the KL divergence [41] from the formulation because it does not embed domain-specific information and replaces it in favor of an augmented view of the original example. Mathematically, this proposed replacement results in the following loss function:

$$J_{\text{AASAE}}(\phi, \psi) = \frac{1}{N} \sum_{n=1}^N \mathbb{E}_{x_n^+ \sim A(x_n)} [\mathbb{E}_{z \sim q_\phi(z_n|x_n^+)} [\log p_\psi(x_n|z_n)]], \quad (3)$$

where $A = (a_1, a_2, \dots, a_n)$ is a stochastic process that applies a sequence of stochastic input transformations a_n . A transforms any input x to generate a view $x^+ \sim A(x)$, while preserving the major semantic characteristics of x .

The proposed replacement effectively works by forcing the encoder of the AASAE to put representations of different views of each example close to each other since the original example must be reconstructed from all of them. This is unlike the original KL divergence term, which packs the representations globally into the prior. In other words, we replace this global packing with the local packing, where the domain-specific transformations define the local neighborhood. Furthermore, domain-aware transformations have the effect of filling in the gaps between training examples, which indirectly achieves the goal of global packing.

Comparison to existing approaches Compared to the existing approaches, both contrastive and non-contrastive ones, the AASAE has a unique advantage. AASAE’s loss function is decomposed over the examples, which avoids the need of approximating data-level statistics and computing its gradient for learning. This is advantageous, because we know precisely what we are computing when we use a small minibatch to approximate the gradient of the whole loss function. Generally, this is not the case with algorithms where we need to approximate the gradient of data-level statistics using a small mini-batch. Based on this observation, we expect our approach to be robust to the minibatch size, which we later confirm experimentally in the paper.

A relatively minor but related advantage of the proposed approach over contrastive learning is that there is no need to design a strategy for selecting negatives for each training example. Considering a flurry of recent work reporting on the importance of mining better negative examples [54, 10, 51], our approach based on autoencoding greatly simplifies self-supervised learning by entirely eliminating negative examples.

4 Experiments

4.1 Setup

Architecture The encoder ϕ in our experiments is composed of a residual network backbone [30] followed by a projection layer similar to the one described in [7]. The decoder ψ is an inverted version of residual backbone with its batch normalization [36] layers removed. We use Resnet-50 as a default option for both the encoder and decoder, but later experiment with varying the decoder architecture.

Datasets We test the proposed AASAE and other more conventional autoencoder models by pretraining them on three datasets: CIFAR-10 [40], STL-10 [11] and Imagenet [13]. CIFAR-10 consists of 50,000 32x32 images in the training set and 10,000 images in the test set. These images are equally divided across 10 labeled classes. For pretraining we use 45,000 image from the training set while 5,000 images are kept for validation. The STL-10 dataset consists of 100,000 unlabelled images resized to 96x96 which are split into 95,000 images for self-supervised pretraining and 5,000 for validation. It further consists of 5,000 training images and 8,000 test images that are labelled across 10 classes. We split the 5,000 training images into 4,500 images for training the downstream classification task and the remaining 500 are kept for validation. Imagenet consists of 1.2 million images in the training split and 50,000 images in the validation split, spread across 1000 classes. We separate 5000 images from the training set to create our own validation set for finetuning the hyperparameters. The official validation set of Imagenet is what we report the final results on.

Augmentation pipeline As mentioned in the paragraph above, we choose image datasets for our experiments with AASAEs, and hence setup the denoising criterion with an appropriate domain-specific data augmentation pipeline. We define a sequence of common image augmentations $A = \{a_1, a_2, \dots, a_n\}$ such as random flip, random channel drop. We also define a_c as a special transform that applies a random resize and crop to an input x . Formally, a_c maps $x : \mathbb{R}^{c \times h \times w} \rightarrow \mathbb{R}^{c \times g \times u}$ where $g \leq h$ and $u \leq w$. For every input x to a AASAE we define $x^+ \sim A(a_c(x))$ as a view of x . The augmentation pipeline defined here is kept the same as that of SimCLR [7], for a fair comparison with other self-supervised learning approaches.

Optimization and Hyperparameters We use Adam optimizer [37] during pretraining. We use a linear warmup schedule for the learning rate, which is held fixed after the initial warmup. For all our ablation experiments, we keep the weight decay coefficient fixed at 0. When studying the effect of minibatch size, we follow [25] and linearly scale the learning rate and the warmup epoch count with minibatch size. For the hyperparameter sensitivity ablations on CIFAR-10, we vary a particular hyperparameter while keeping the others fixed to their default values. By default, we use a learning rate of 2.5×10^{-4} , warmup the learning rate until 10 epochs, and keep the batch size at 256. For STL-10 experiments, we set the learning rate at 5×10^{-4} , warmup epochs count at 10, and keep the batch size at 512. For Imagenet pretraining, we set the total batch size at 512 across 4 GPUs, the learning rate at 5×10^{-4} , warmup epochs count at 10 and run the pretraining for all autoencoder models until 5 million training iterations.

Finetuning Downstream classification accuracy via finetuning has become a widely-used proxy for measuring representation quality. We follow the finetuning protocol put forward by Chen et al. [7]. After pretraining without any labels, we add and train a linear layer on the pretrained encoder (representation), without updating the encoder. We train the linear layer for 90 epochs with a learning rate defined by: $0.1 * \text{BatchSize}/256$, using SGD with Nesterov momentum.

Semi-supervised learning evaluation We run semi-supervised classification task on our models that have been pretrained on the Imagenet dataset. We follow the evaluation process mentioned in previous works [5, 61], and train the model on 1% and 10% labeled splits of Imagenet. The training is carried out for 20 epochs with a batch size of 256, using an SGD optimizer with a momentum of 0.9 and no weight decay. Since this is a semi-supervised learning setup with a certain percentage of labels available from the dataset, the backbone is unfrozen during the training process and is trained at a learning rate of 0.01 for the 10% labeled split and at 0.02 for the 1% labeled split. The linear layer appended on top of the backbone is trained at a learning rate of 0.2 for the 10% labeled split and at a rate of 0.5 for the 1% labeled split.

Transfer learning tasks For the linear classification transfer learning task we use Places205 dataset with the commonly used evaluation protocol [61, 5]. We train a single linear layer on top of our model for 14 epochs with an SGD optimizer with a learning rate of 0.01, momentum of 0.9 and a weight decay of $5e-4$. The learning rate is multiplied by a factor of 0.1 at equally spaced intervals during the training.

For the object detection transfer learning task, we use the VOC07+12 *trainval* set for training and VOC07 test set for eval as previously done by Zbontar et al. [61]. Faster R-CNN with a C4 backbone is used for this downstream task. We train with a batch size of 16 across 8 GPUs for 24000 iterations with a base learning rate of 0.01. We use detectron2 [59] library to perform this evaluation.

Pretraining duration As we demonstrate in the paper, the proposed AASAE benefits from being trained as long as it is feasible. We report the downstream accuracies measured at different points of pretraining. More specifically, we run linear evaluation on our encoder after 400, 800, 1600, and 3200 epochs for the CIFAR-10 experiments. For STL-10, we pretrain our models till 3200 epochs. For Imagenet, we train upto 5 million training steps, which is approximately 2100 epochs.

Compute and Framework All CIFAR-10 [40] experiments are done on a single GPU with a memory size of at least 16GB. All STL-10 experiments are done using two GPUs in the same category. We select GPUs from a mix of NVIDIA RTX 3090s and V100s for CIFAR-10 and STL-10 experiments. Imagenet experiments and downstream evaluations are carried out on 4 A100s. Our codebase uses PyTorch Lightning [20].

Table 1: Classification performance of Resnet-50 [30] backbone on CIFAR-10 [40], STL-10 [11] and Imagenet [13] across different methods. All models were pretrained on the corresponding dataset without labels and finetuned using the protocol described in SimCLR [7]. The autoencoder trained with our denoising criterion (AASAE) outperforms the baseline VAE by 30% on CIFAR-10, 40% on STL-10 and 45% on Imagenet. Methods marked with ♣ either use a different backbone than Resnet-50 or a different (non-linear) evaluation strategy.

Method	CIFAR-10	STL-10	Imagenet	Method	Imagenet
♣ CPC (large)	-	-	48.7	Colorization	39.6
♣ CPCv2	84.52	78.36	63.8	Rotation	48.9
♣ AMDIM (small)	92.10	91.50	63.5	Jigsaw	45.7
♣ YADIM	91.30	92.15	59.19	BigBiGAN	56.6
SIMCLR	94.00	92.36	69.3	NPID	54.0
AE	56.34	42.26	0.89	MoCo	60.6
AAAE	50.62	41.94	1.29	SwAV	75.3
VAE	57.16	44.15	4.58	BYOL	74.3
AASAE	87.14	84.72	51.0	Barlow Twins	73.2

4.2 Quality of representation: downstream classification accuracies

First, we look at the accuracies from variants of autoencoders, the family to which the proposed AASAE belongs, presented in the bottom half of Table 1 (left). We consider the vanilla autoencoder (AE), augmentation-augmented autoencoder (AAAE), and the variational autoencoder (VAE) as baselines. Our first observation is that there is a significant gap between the proposed AASAE and all the baselines, with up to 30% points on CIFAR-10, 40% points on STL-10, and 45% points on Imagenet. This demonstrates the importance of data augmentation and noise in the intermediate representation space in making autoencoding a competitive alternative for self-supervised learning. When we add only one of these components, augmentation in the case of AAAEs or sampling in the case of VAEs, we see a big performance degradation from AASAE. The gap between VAE and AASAE exposes the inadequacy of KL-divergence as a regularizer for the latent space.

We then put the performance of the proposed AASAE in the context of existing self-supervised learning algorithms presented in the top half of Table 1 (left), and Table 1 (right). We confirm once again what others have observed as to why autoencoding fell out of interest in recent years. All three autoencoder baselines (AE, AAAE, and VAE) severely lag behind the other state-of-the-art self-supervised learning approaches. However, the proposed modification that led to AASAE significantly narrows this gap on CIFAR-10 and STL-10. On Imagenet, the AASAE lags behind the current crop of state-of-the-art methods; however, it performs better than any existing pretext task designed for SSL. These results suggest that autoencoding is a viable alternative to contrastive and non-contrastive learning algorithms when designed and equipped appropriately and developed further on from here.

4.3 Representational quality does not deteriorate

A major downside of the proposed strategy of replacing the KL divergence term in the original loss with data augmentation is that we lose the interpretation of the negative loss as the lowerbound to the log probability of an observation. However, we find it less concerning as the quality of representation is not necessarily equivalent to the quality of density estimation. Furthermore, we make a strong conjecture that the representation quality, which largely depends on the encoder, does not suffer from overfitting (in terms of downstream classification accuracy), even when the quality of density estimation does. Our conjecture comes from the observations that the representation output of the encoder must cope with multiple copies of the same input and noise added in the process of sampling. On the other hand, the decoder can arbitrarily shrink the width of the output distribution per latent configuration, resulting in overfitting to training examples. This conjecture is important since it implies that we should train the AASAE as long as the computational budget allows, rather than introducing a sophisticated early stopping criterion. More importantly, this would also imply that we do not need to assume the availability of downstream tasks at the time of pretraining.

We test two setups. First, we let the decoder determine the width (in terms of the diagonal covariance of Gaussian) on its own. In this case, we expect the model to overfit the training examples severely, as was observed and argued by Mattei and Frellsen [42], while the representation quality never

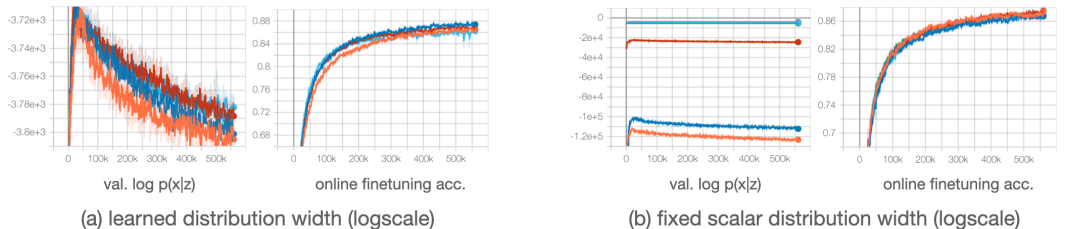


Figure 2: The AASAE uses a Gaussian likelihood on pixels for the reconstruction loss with a specified width of the distribution (logscale). In (a), we let the decoder learn the logscale and observe the illusion of overfitting as mentioned in Mattei and Frellsen [42]. In (b), we fix the logscale parameter to an arbitrary scalar by sampling uniformly between $[-5, 2]$. In both cases, we fail to observe any correlation between the quality of density estimation and learned representation. Plots shown for CIFAR-10 [40] dataset.

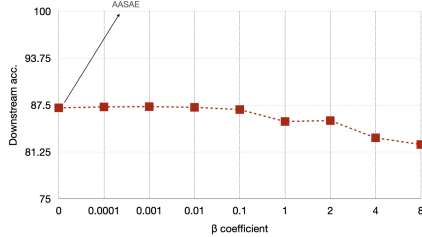


Figure 3: Downstream classification accuracy on CIFAR-10 [40] when we add back KL divergence based regularization with a β -coefficient [33] to the loss function of AASAE defined in Eq. 3. We observe a negligible change in the quality of representations, as measured by the classification task, when the KL-term is weighted with a $\beta \ll 1$. For values of $\beta \geq 1$, the quality of representation starts deteriorating, as is seen by the decrease in classification accuracy.

deteriorates. In the second setup, we fix the width to an arbitrary but reasonable scalar, which would prevent overfitting in the context of density estimation as long as it is chosen to be reasonably large.

As presented in Fig. 2, in both cases, we observe that the quality of representation, measured in terms of the downstream accuracy, does not deteriorate. Furthermore, as anticipated, we observe that the quality of density estimation quickly overfits in learning the width of output distribution (Figure 2 (a)). Fixing the width to a scalar did not necessarily help avoid the issue of overfitting (Figure 2 (b)). Still, more importantly, we fail to observe any clear relationship between the qualities of density estimation and learned representation.

This finding suggests the need for further study to define and measure the quality of representation distinct from both density estimation quality and downstream accuracy. The former will not only help us measure the learning progress in pretraining time, but will also shed light on what we mean by representation and representation learning. The latter will be needed for future downstream tasks, as the main promise of pretraining is that it results in representations that are useful in the unknown.

4.4 Combining VAE and AASAE

Although we designed AASAE by *replacing* the KL divergence based regularization with data augmentation based denoising, these two may well be used together. Earlier, Im Im et al. [35] studied this combination with a simple corruption distribution that is agnostic to the input domain in the context of density estimation. Here, we investigate this combination, with domain-specific transformations, in the context of representation quality.

While keeping the data augmentation based perturbation scheme intact, we vary the coefficient β of the KL divergence term. When $\beta = 0$, it is equivalent to the proposed AASAE. We present the downstream classification accuracies on CIFAR-10 in Figure 3.

We first observe that the KL divergence term has negligible impact when the coefficient is small, i.e., $\beta \ll 1$. However, as β grows, we notice a significant drop in the downstream classification accuracy, which we view as a proxy to the representation quality. We attribute this behavior to the tension, or balance, between domain-aware and domain-agnostic regularization of the representation space. As $\beta \rightarrow \infty$, the domain-agnostic regularization overtakes and results in the arrangement of the representations that does not reflect the domain-specific structures, leading to worse downstream classification accuracy.

From this experiment, we conclude that for self-supervised pretraining, the proposed approach of data augmentation is a better way to shape the representation space than the domain-agnostic KL divergence based regularization.

4.5 Hyperparameter sensitivity

The proposed AASAE, or even the original VAE, sets itself apart from the recently proposed self-supervised learning methods in that its loss function is decomposed over the training examples (within each minibatch.) Thus, we believe that training the AASAE is less sensitive to minibatch size, as even with a single-example minibatch, our estimate of the gradient is unbiased. This is often

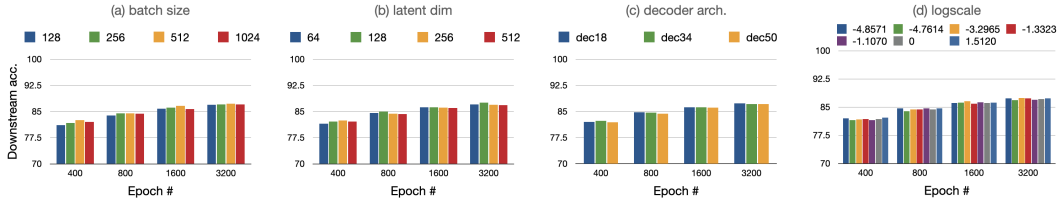


Figure 4: On CIFAR-10 [40], we demonstrate AASAEs insensitivity to hyperparameters: (a) batch size, (b) latent space dimension, (c) decoder architecture, and (d) logscale parameter (width of the Gaussian likelihood). We vary one specific hyperparameter while keeping the rest fixed for these insensitivity ablations. We select the minibatch size between 128-1024, the dimensionality of the latent space between 64-512, the decoder architecture from decoders that mirror {resnet18, resnet34 or resnet50} encoders, and sample the logscale values from a uniform distribution between [-5, 2].

not guaranteed for a loss function that is not decomposed over the training examples. We test this hypothesis by running experiments with varying sizes of minibatches.

As shown in Fig. 4 (a), we observe almost no difference across different minibatch sizes, spanning from 128 to 1024. This is true for both the downstream accuracy (representation quality) and the speed of learning. This is contrary to recent findings from self-supervised learning algorithms, where large minibatches have been identified as an important ingredient [7, 55].

This insensitivity to the minibatch size raises a question about other hyperparameters, such as the dimensionality of latent space (Fig. 4 (b)), the decoder architecture (Fig. 4 (c)) and the logscale or width of the output distribution (Fig. 4 (d)). We test the sensitivity of the proposed AASAE to each of these hyperparameters. We find that the quality of representation, measured by the downstream classification accuracy, is largely constant to the change in these hyperparameters. Together with the insensitivity to the minibatch size, this finding further supports our claim that autoencoding-based approaches form a valuable addition to self-supervised learning.

4.6 Semi-supervised learning

We finetune the Resnet-50 [30] backbone pretrained by AASAEs on specified labeled subsets of Imagenet. The two subsets used contain 1% and 10% labeled images of the total number present in the dataset. Table 2 shows the results for the baseline autoencoder models and our proposed AASAE. The baseline autoencoders are pretty poor in their performance for this semi-supervised evaluation task. In some instances, their performance is 0.1% accuracy on Imagenet, which is equivalent to chance. The AASAE outperforms the remaining autoencoders considerably on this task with 21.37% accuracy on the 1% labeled subset and a 39.85% accuracy on the 10% labeled subset. However, this is still quite behind when compared against the supervised results or results from other current SSL methods.

Table 2: Semi-supervised evaluation of Resnet-50 encoder with 1% and 10% labels on Imagenet. Entries with * next to them performed equivalent to chance result on for Imagenet.

Method	Imagenet	
	1%	10%
Supervised	25.4	56.4
SimCLR	48.3	65.6
Barlow Twins	55.0	69.7
BYOL	53.2	68.8
AE	0.1*	0.1*
AAAE	0.1*	0.31
VAE	0.1*	0.98
AASAE	21.37	39.85

Table 3: Transfer performance of Imagenet pretrained Resnet-50 backbones on classification and object detection tasks. Places205 dataset is used for classification transfer task with the table reporting classification accuracy. For object detection, we use VOC07+12 dataset with Faster R-CNN algorithm and C4 backbone.

Method	Places205		VOC07+12	
	<i>Acc.</i>	<i>AP_{all}</i>	<i>AP₅₀</i>	<i>AP₇₅</i>
Supervised	51.1	53.5	81.3	58.8
Jigsaw	41.2	48.9	75.1	52.9
Rotation	41.4	46.3	72.5	49.3
Barlow Twins	54.1	56.8	82.6	63.4
VAE	6.78	2.45	6.49	1.67
AASAE	41.45	15.22	35.69	10.09

4.7 Transfer learning to other tasks

For transfer learning to classification tasks, we finetune a linear layer on top of the frozen Resnet-50 backbone pretrained by VAE and AASAE on Places205 dataset for scene classification. The finetuning protocol is kept the same as the previous works of Zbontar et al. [61], Misra and van der Maaten [43]. Table 3 shows the results for this downstream evaluation. For comparison, we also include results on Places205 from pretext tasks of Jigsaw [45] and Rotation [23], while at the same time including results from one of the current high performers on this evaluation, namely, Barlow Twins [61].

The finetuning process of object detection transfer task is done on VOC07+12 *trainval* dataset and the task is evaluated on VOC07 test set. The results are shown in Table 3. Even though the AASAE performed comparable to the Jigsaw and Rotation pretext tasks on Places205 classification, its performance is greatly affected on the VOC07 detection task. It is far behind the results of these pretext tasks. This result asks whether reconstruction-based SSL techniques are a good fit for transferring representations for object detection tasks. This is something that can be explored in future work.

4.8 Direct inspection of representation

A major motivation behind our proposal was to use domain-specific data augmentation to encourage representations to encode domain-specific invariances. If AASAEs indeed reflect such invariances, we expect vector representations coming out of domain-specific perturbations of an individual example to be highly aligned with each other. We test whether this property holds with the AASAE more strongly than the original VAE by inspecting cosine similarities between pairs of perturbed inputs produced by the same example and between pairs of perturbed inputs produced by different examples.

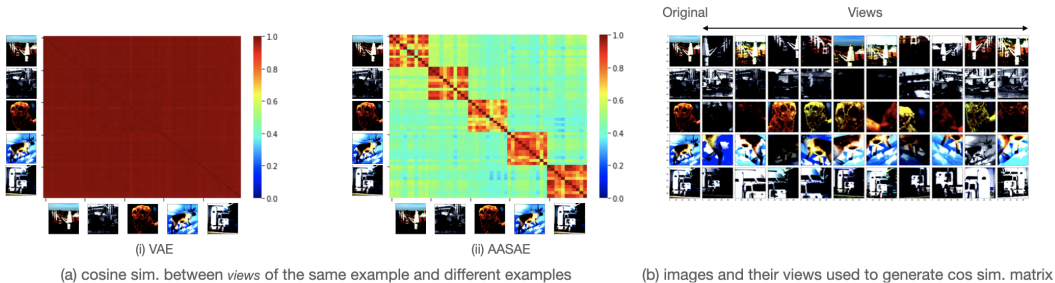


Figure 5: Part (a) shows cosine similarity matrices between pairs of vectors produced by views of a particular example and between pairs of vectors produced by views of different examples. We observe a posterior collapse in the case of VAEs in (a)(i). For AASAEs in (a)(ii), we see strong alignment between views of the same example while the views of different examples are far apart from each other in the representation space. In (b), we show images from the STL-10 dataset [11] and their corresponding perturbed versions that generate the cosine similarity matrices in (a).

When the former is higher than the latter, we can say the representation encodes domain-specific invariances induced by data augmentation.

In Fig. 5 (a)(i), we make two observations. First, the representation vectors are all extremely aligned for the original VAE. We can interpret this from two perspectives. The first perspective is the so-called posterior collapse [33, 15], in which all the approximate posterior distributions, i.e., the representation vectors, are detached from the input and collapse onto each other. The second perspective is the lack of domain-specific invariance, which is evident from the lack of any clusters. Either way, it is obvious that the representations extracted by the original VAE do not reflect the underlying structure of the data well.

On the other hand, with the proposed AASAE, we see clear patterns of clustering in Fig. 5 (a)(ii). The vectors produced from one example are highly aligned with each other, while the vectors produced from two different examples are less aligned. In other words, the representations capture domain-specific invariances, induced by data augmentation, and the AASAE does not suffer from posterior collapse. Both these things were well anticipated from the design of our algorithm.

5 Conclusion

In this paper, we attempt to revive the idea of autoencoding for self-supervised learning of representations. We start by observing that data augmentation is at the core of all recently successful self-supervised learning algorithms, including both contrastive and non-contrastive approaches. We then identify the KL divergence in variational autoencoders (VAE) as a domain-agnostic way of shaping the representation space and hypothesize that this makes it inadequate for representation learning. Based on these two observations: the importance of data augmentations and KL divergence’s inadequacy, we propose replacing the KL divergence regularizer with a denoising criterion and domain-specific data augmentations in the VAE and call this variant an augmentation-augmented stochastic autoencoder (AASAE).

Our experiments reveal that the AASAE learns substantially better data representation than the original VAE or any other conventional variant, including the vanilla autoencoder and the augmentation-augmented denoising autoencoder. We use downstream classification accuracy from finetuning a linear layer as the metric to measure representation quality and observe more than a 30% improvement on all datasets over the VAE. This result is better than any pretext task for SSL and one of the earlier versions of contrastive learning, CPC. Although the AASAE still lags behind the more recent methods for SSL, this gap is significantly narrower with the AASAE than with any other autoencoding variant.

One consequence of autoencoding is that the loss function of AASAE is decomposed over the examples within each minibatch, unlike contrastive learning (with negative examples from the same minibatch) and non-contrastive learning (which often relies on minibatch statistics). We anticipated that this makes AASAE learning less sensitive to various hyperparameters, especially the minibatch size. Our experiments reveal that the AASAE is indeed insensitive to the minibatch size, latent space dimension, and decoder architecture.

Although the proposed AASAE has failed to outperform or perform comparably to the existing families of self-supervised learning algorithms, our experiments indicate the potential for the third category of self-supervised learning algorithm based on autoencoding. The quality of representations can be significantly pushed beyond that of the vanilla autoencoder and variational autoencoder by making them encode domain specific invariances. Furthermore, autoencoding-based methods, represented by the AASAE, are robust to the choice of hyperparameters. Based on these observations, we advocate for further research in the direction of autoencoding-based self-supervised learning.

Acknowledgments and Disclosure of Funding

Ananya Harsh thanks Margaret Li, Tushar Jain, Jiri Bovec, Thomas Chaton and Marc Ferradou for helpful discussions on ideas, experiments and the paper draft. William thanks Yann LeCun, Philip Bachman, Carl Doersch, Cinjon Resnick, Tullie Murrell for helpful discussions.

We are grateful to the PyTorch Lightning team for their support of this project and Grid AI for providing compute resources and cloud credits needed to run our research workloads at scale. We

thank the PyTorch team and the PyTorch Lightning community for their contributions to PyTorch, Lightning and Bolts which made the code base for this project possible.

KC was partly supported by NSF Award 1922658 NRT-HDR: FUTURE Foundations, Translation, and Responsibility for Data Science.

References

- [1] Y. M. Asano, C. Rupprecht, and A. Vedaldi. Self-labelling via simultaneous clustering and representation learning. *CoRR*, abs/1911.05371, 2019. URL <http://arxiv.org/abs/1911.05371>.
- [2] P. Bachman, R. D. Hjelm, and W. Buchwalter. Learning representations by maximizing mutual information across views. In H. M. Wallach, H. Larochelle, A. Beygelzimer, F. d’Alché-Buc, E. B. Fox, and R. Garnett, editors, *Advances in Neural Information Processing Systems 32: Annual Conference on Neural Information Processing Systems 2019, NeurIPS 2019, December 8-14, 2019, Vancouver, BC, Canada*, pages 15509–15519, 2019.
- [3] A. Bardes, J. Ponce, and Y. LeCun. Vicreg: Variance-invariance-covariance regularization for self-supervised learning. *CoRR*, abs/2105.04906, 2021. URL <https://arxiv.org/abs/2105.04906>.
- [4] M. Caron, P. Bojanowski, A. Joulin, and M. Douze. Deep clustering for unsupervised learning of visual features. *CoRR*, abs/1807.05520, 2018. URL <http://arxiv.org/abs/1807.05520>.
- [5] M. Caron, I. Misra, J. Mairal, P. Goyal, P. Bojanowski, and A. Joulin. Unsupervised learning of visual features by contrasting cluster assignments. *arXiv preprint arXiv:2006.09882*, 2020.
- [6] M. Caron, H. Touvron, I. Misra, H. Jégou, J. Mairal, P. Bojanowski, and A. Joulin. Emerging properties in self-supervised vision transformers. *CoRR*, abs/2104.14294, 2021. URL <https://arxiv.org/abs/2104.14294>.
- [7] T. Chen, S. Kornblith, M. Norouzi, and G. E. Hinton. A simple framework for contrastive learning of visual representations. In *Proceedings of the 37th International Conference on Machine Learning, ICML 2020, 13-18 July 2020, Virtual Event*, volume 119 of *Proceedings of Machine Learning Research*, pages 1597–1607. PMLR, 2020. URL <http://proceedings.mlr.press/v119/chen20j.html>.
- [8] X. Chen and K. He. Exploring simple siamese representation learning. *CoRR*, abs/2011.10566, 2020. URL <https://arxiv.org/abs/2011.10566>.
- [9] X. Chen, H. Fan, R. B. Girshick, and K. He. Improved baselines with momentum contrastive learning. *CoRR*, abs/2003.04297, 2020. URL <https://arxiv.org/abs/2003.04297>.
- [10] C. Chuang, J. Robinson, Y. Lin, A. Torralba, and S. Jegelka. Debaised contrastive learning. In H. Larochelle, M. Ranzato, R. Hadsell, M. Balcan, and H. Lin, editors, *Advances in Neural Information Processing Systems 33: Annual Conference on Neural Information Processing Systems 2020, NeurIPS 2020, December 6-12, 2020, virtual*, 2020. URL <https://proceedings.neurips.cc/paper/2020/hash/63c3ddcc7b23daa1e42dc41f9a44a873-Abstract.html>.
- [11] A. Coates, A. Ng, and H. Lee. An analysis of single-layer networks in unsupervised feature learning. *Proceedings of the Fourteenth International Conference on Artificial Intelligence and Statistics*, PMLR 15:215–223, 2011.
- [12] M. Cuturi. Sinkhorn distances: Lightspeed computation of optimal transport. In C. J. C. Burges, L. Bottou, M. Welling, Z. Ghahramani, and K. Q. Weinberger, editors, *Advances in Neural Information Processing Systems*, volume 26. Curran Associates, Inc., 2013. URL <https://proceedings.neurips.cc/paper/2013/file/af21d0c97db2e27e13572cbf59eb343d-Paper.pdf>.
- [13] J. Deng, W. Dong, R. Socher, L.-J. Li, K. Li, and L. Fei-Fei. Imagenet: A large-scale hierarchical image database. In *2009 IEEE Conference on Computer Vision and Pattern Recognition*, pages 248–255, 2009. doi: 10.1109/CVPR.2009.5206848.
- [14] V. R. DeSa. Learning classification with unlabeled data. In *NIPS 1993*, 1993.
- [15] A. B. Dieng, Y. Kim, A. M. Rush, and D. M. Blei. Avoiding latent variable collapse with generative skip models. In K. Chaudhuri and M. Sugiyama, editors, *The 22nd International Conference on Artificial Intelligence and Statistics, AISTATS 2019, 16-18 April 2019, Naha, Okinawa, Japan*, volume 89 of *Proceedings of Machine Learning Research*, pages 2397–2405. PMLR, 2019. URL <http://proceedings.mlr.press/v89/dieng19a.html>.
- [16] C. Doersch and A. Zisserman. Multi-task self-supervised visual learning. *CoRR*, abs/1708.07860, 2017. URL <http://arxiv.org/abs/1708.07860>.

- [17] C. Doersch, A. Gupta, and A. A. Efros. Unsupervised visual representation learning by context prediction. In *2015 IEEE International Conference on Computer Vision, ICCV 2015, Santiago, Chile, December 7-13, 2015*, pages 1422–1430. IEEE Computer Society, 2015. doi: 10.1109/ICCV.2015.167. URL <https://doi.org/10.1109/ICCV.2015.167>.
- [18] M. Donsker and S. Varadhan. Asymptotic evaluation of certain markov process expectations for large time, iv. *Communications on Pure and Applied Mathematics*, 36(2):183–212, 1983.
- [19] W. Falcon and K. Cho. A framework for contrastive self-supervised learning and designing a new approach. *arXiv preprint arXiv:2009.00104*, 2020.
- [20] W. Falcon et al. Pytorch lightning. *GitHub. Note: <https://github.com/PyTorchLightning/pytorch-lightning>*, 3, 2019.
- [21] R. A. Fisher. The use of multiple measures in taxonomic problems. *Annals of Eugenics*, 7: 179–188, 1936.
- [22] A. Genevay, G. Peyré, and M. Cuturi. Learning generative models with sinkhorn divergences. In A. J. Storkey and F. Pérez-Cruz, editors, *International Conference on Artificial Intelligence and Statistics, AISTATS 2018, 9-11 April 2018, Playa Blanca, Lanzarote, Canary Islands, Spain*, volume 84 of *Proceedings of Machine Learning Research*, pages 1608–1617. PMLR, 2018. URL <http://proceedings.mlr.press/v84/genevay18a.html>.
- [23] S. Gidaris, P. Singh, and N. Komodakis. Unsupervised representation learning by predicting image rotations. *CoRR*, abs/1803.07728, 2018. URL <http://arxiv.org/abs/1803.07728>.
- [24] S. Gidaris, A. Bursuc, G. Puy, N. Komodakis, M. Cord, and P. Pérez. Online bag-of-visual-words generation for unsupervised representation learning. *CoRR*, abs/2012.11552, 2020. URL <https://arxiv.org/abs/2012.11552>.
- [25] P. Goyal, P. Dollár, R. B. Girshick, P. Noordhuis, L. Wesolowski, A. Kyrola, A. Tulloch, Y. Jia, and K. He. Accurate, large minibatch SGD: training imagenet in 1 hour. *CoRR*, abs/1706.02677, 2017. URL <http://arxiv.org/abs/1706.02677>.
- [26] P. Goyal, D. Mahajan, A. Gupta, and I. Misra. Scaling and benchmarking self-supervised visual representation learning. In *2019 IEEE/CVF International Conference on Computer Vision, ICCV 2019, Seoul, Korea (South), October 27 - November 2, 2019*, pages 6390–6399. IEEE, 2019. doi: 10.1109/ICCV.2019.00649. URL <https://doi.org/10.1109/ICCV.2019.00649>.
- [27] P. Goyal, M. Caron, B. Lefauveux, M. Xu, P. Wang, V. Pai, M. Singh, V. Liptchinsky, I. Misra, A. Joulin, and P. Bojanowski. Self-supervised pretraining of visual features in the wild. *CoRR*, abs/2103.01988, 2021. URL <https://arxiv.org/abs/2103.01988>.
- [28] J.-B. Grill, F. Strub, F. Altché, C. Tallec, P. H. Richemond, E. Buchatskaya, C. Doersch, B. A. Pires, Z. D. Guo, M. G. Azar, et al. Bootstrap your own latent: A new approach to self-supervised learning. *arXiv preprint arXiv:2006.07733*, 2020.
- [29] R. Hadsell, S. Chopra, and Y. LeCun. Dimensionality reduction by learning an invariant mapping. In *2006 IEEE Computer Society Conference on Computer Vision and Pattern Recognition (CVPR'06)*, volume 2, pages 1735–1742, 2006. doi: 10.1109/CVPR.2006.100.
- [30] K. He, X. Zhang, S. Ren, and J. Sun. Deep residual learning for image recognition. In *Proceedings of the IEEE conference on computer vision and pattern recognition*, pages 770–778, 2016.
- [31] K. He, H. Fan, Y. Wu, S. Xie, and R. B. Girshick. Momentum contrast for unsupervised visual representation learning. In *2020 IEEE/CVF Conference on Computer Vision and Pattern Recognition, CVPR 2020, Seattle, WA, USA, June 13-19, 2020*, pages 9726–9735. IEEE, 2020. doi: 10.1109/CVPR42600.2020.00975. URL <https://doi.org/10.1109/CVPR42600.2020.00975>.
- [32] O. J. Hénaff, A. Srinivas, J. D. Fauw, A. Razavi, C. Doersch, S. M. A. Eslami, and A. van den Oord. Data-efficient image recognition with contrastive predictive coding. *CoRR*, abs/1905.09272, 2019.
- [33] I. Higgins, L. Matthey, A. Pal, C. Burgess, X. Glorot, M. Botvinick, S. Mohamed, and A. Lerchner. beta-vae: Learning basic visual concepts with a constrained variational framework. 2016.

- [34] R. D. Hjelm, A. Fedorov, S. Lavoie-Marchildon, K. Grewal, A. Trischler, and Y. Bengio. Learning deep representations by mutual information estimation and maximization. *arXiv preprint arXiv:1808.06670*, 2018.
- [35] D. Im Im, S. Ahn, R. Memisevic, and Y. Bengio. Denoising criterion for variational auto-encoding framework. In *Proceedings of the AAAI Conference on Artificial Intelligence*, volume 31, 2017.
- [36] S. Ioffe and C. Szegedy. Batch normalization: Accelerating deep network training by reducing internal covariate shift. In *International conference on machine learning*, pages 448–456. PMLR, 2015.
- [37] D. P. Kingma and J. Ba. Adam: A method for stochastic optimization. *arXiv preprint arXiv:1412.6980*, 2014.
- [38] D. P. Kingma and M. Welling. Auto-encoding variational bayes. *arXiv preprint arXiv:1312.6114*, 2013.
- [39] I. Kostrikov, D. Yarats, and R. Fergus. Image augmentation is all you need: Regularizing deep reinforcement learning from pixels. *CoRR*, abs/2004.13649, 2020. URL <https://arxiv.org/abs/2004.13649>.
- [40] A. Krizhevsky and G. Hinton. Learning multiple layers of features from tiny images. *Technical report, Citeseer*, 1, 2009.
- [41] S. Kullback and R. A. Leibler. On information and sufficiency. *The annals of mathematical statistics*, 22(1):79–86, 1951.
- [42] P.-A. Mattei and J. Frellsen. Leveraging the exact likelihood of deep latent variable models. *arXiv preprint arXiv:1802.04826*, 2018.
- [43] I. Misra and L. van der Maaten. Self-supervised learning of pretext-invariant representations. In *2020 IEEE/CVF Conference on Computer Vision and Pattern Recognition, CVPR 2020, Seattle, WA, USA, June 13-19, 2020*, pages 6706–6716. IEEE, 2020. doi: 10.1109/CVPR42600.2020.00674. URL <https://doi.org/10.1109/CVPR42600.2020.00674>.
- [44] N. Ng, K. Cho, and M. Ghassemi. SSMBA: self-supervised manifold based data augmentation for improving out-of-domain robustness. *CoRR*, abs/2009.10195, 2020. URL <https://arxiv.org/abs/2009.10195>.
- [45] M. Noroozi and P. Favaro. Unsupervised learning of visual representations by solving jigsaw puzzles. *CoRR*, abs/1603.09246, 2016. URL <http://arxiv.org/abs/1603.09246>.
- [46] S. Nowozin, B. Cseke, and R. Tomioka. f-gan: Training generative neural samplers using variational divergence minimization, 2016.
- [47] A. v. d. Oord, Y. Li, and O. Vinyals. Representation learning with contrastive predictive coding. *arXiv preprint arXiv:1807.03748*, 2018.
- [48] D. Pathak, P. Krähenbühl, J. Donahue, T. Darrell, and A. A. Efros. Context encoders: Feature learning by inpainting. *CoRR*, abs/1604.07379, 2016. URL <http://arxiv.org/abs/1604.07379>.
- [49] R. Raileanu, M. Goldstein, D. Yarats, I. Kostrikov, and R. Fergus. Automatic data augmentation for generalization in deep reinforcement learning. *CoRR*, abs/2006.12862, 2020. URL <https://arxiv.org/abs/2006.12862>.
- [50] P. H. Richemond, J.-B. Grill, F. Altché, C. Tallec, F. Strub, A. Brock, S. Smith, S. De, R. Pascanu, B. Piot, and M. Valko. Byol works even without batch statistics, 2020.
- [51] J. D. Robinson, C. Chuang, S. Sra, and S. Jegelka. Contrastive learning with hard negative samples. In *9th International Conference on Learning Representations, ICLR 2021, Virtual Event, Austria, May 3-7, 2021*. OpenReview.net, 2021. URL <https://openreview.net/forum?id=CR1X0QOUTH->.
- [52] A. Tarvainen and H. Valpola. Weight-averaged consistency targets improve semi-supervised deep learning results. *CoRR*, abs/1703.01780, 2017. URL <http://arxiv.org/abs/1703.01780>.
- [53] Y. Tian, D. Krishnan, and P. Isola. Contrastive multiview coding. *CoRR*, abs/1906.05849, 2019. URL <http://arxiv.org/abs/1906.05849>.

- [54] Y. Tian, C. Sun, B. Poole, D. Krishnan, C. Schmid, and P. Isola. What makes for good views for contrastive learning? In H. Larochelle, M. Ranzato, R. Hadsell, M. Balcan, and H. Lin, editors, *Advances in Neural Information Processing Systems 33: Annual Conference on Neural Information Processing Systems 2020, NeurIPS 2020, December 6-12, 2020, virtual*, 2020. URL <https://proceedings.neurips.cc/paper/2020/hash/4c2e5eaae9152079b9e95845750bb9ab-Abstract.html>.
- [55] Y. Tian, L. Yu, X. Chen, and S. Ganguli. Understanding self-supervised learning with dual deep networks. *CoRR*, abs/2010.00578, 2020. URL <https://arxiv.org/abs/2010.00578>.
- [56] P. Vincent, H. Larochelle, Y. Bengio, and P.-A. Manzagol. Extracting and composing robust features with denoising autoencoders. In *ICML*, pages 1096–1103, 2008. URL <https://doi.org/10.1145/1390156.1390294>.
- [57] P. Vincent, H. Larochelle, I. Lajoie, Y. Bengio, P.-A. Manzagol, and L. Bottou. Stacked denoising autoencoders: Learning useful representations in a deep network with a local denoising criterion. *Journal of machine learning research*, 11(12), 2010.
- [58] K. Weinberger, J. Blitzer, and L. Saul. Distance metric learning for large margin nearest neighbor classification. In *Advances in neural information processing systems*, pages 1473–1480, 2006.
- [59] Y. Wu, A. Kirillov, F. Massa, W.-Y. Lo, and R. Girshick. Detectron2. <https://github.com/facebookresearch/detectron2>, 2019.
- [60] Z. Wu, Y. Xiong, S. X. Yu, and D. Lin. Unsupervised feature learning via non-parametric instance-level discrimination. *CoRR*, abs/1805.01978, 2018. URL <http://arxiv.org/abs/1805.01978>.
- [61] J. Zbontar, L. Jing, I. Misra, Y. LeCun, and S. Deny. Barlow twins: Self-supervised learning via redundancy reduction. *CoRR*, abs/2103.03230, 2021. URL <https://arxiv.org/abs/2103.03230>.
- [62] R. Zhang, P. Isola, and A. A. Efros. Colorful image colorization. In B. Leibe, J. Matas, N. Sebe, and M. Welling, editors, *Computer Vision - ECCV 2016 - 14th European Conference, Amsterdam, The Netherlands, October 11-14, 2016, Proceedings, Part III*, volume 9907 of *Lecture Notes in Computer Science*, pages 649–666. Springer, 2016. doi: 10.1007/978-3-319-46487-9_40. URL https://doi.org/10.1007/978-3-319-46487-9_40.